Influence of Surface Orientation on Oxidation Resistance of Ni-based Single Crystal Superalloy CM186LC at 1100°C in Air

Fahamsyah H. Latief[*], Koji Kakehi, Xintao Fu

Department of Mechanical Engineering, Tokyo Metropolitan University, 1-1 Minami-osawa, Hachioji-shi, Tokyo 192-0397, Japan
[*]E-mail: fahamsyah78@gmail.com

The influence of surface orientation on the oxidation resistance of Ni-based single crystal superalloy CM186LC at 1100°C in air was investigated. The specimens with (001) surface showed a higher oxidation rate value compared to the specimens with (011) surface. This occurrence is primarily due to the number of short-circuit diffusion paths. The specimens with (001) surface formed more diffusion paths than those of (011) surface. The short circuit diffusion paths were produced because of the oxide scales were subjected to an epitaxial-growth force during its growth on surfaces of single crystal alloys during isothermal oxidation. As a consequence, the different specimen surfaces revealed various oxidation rates. In addition, the anisotropy on oxidation resistance can be also evaluated from the difference in thickness of the oxide scale formed on the surface of superalloy CM186LC.

Keywords: Ni-based superalloy, oxidation behavior, microstructure, crystallographic orientation

1. INTRODUCTION

Since the last two decades, Nickel-based single crystal superalloys have been extensively used in turbine blades of industrial gas turbines and jet engines. The materials with excellent properties in mechanical strength and oxidation resistance are required to be applied for such applications [1-3]. Recently, the surface operating temperatures of gas-turbine blades could reach 1150°C or even higher. However, high operating temperature accommodates the degradation of superalloys during service with respect to oxidation or corrosion [4,5]. For materials used at high temperature applications, the oxidation behavior of materials becomes one of the predominant life-limiting factors.

In order to improve the mechanical properties of superalloys, several alloying elements are usually added, including Mo, W, Ta, Re and Nb through the solid solution hardening method and Al and Ta via formation of a γ′ precipitate in a γ nickel matrix [6,7]. The superalloys with refractory

elements containing have a good protection to local hot corrosion and Re addition are believed to improve the oxidation resistance as well [8]. Sometimes, carbon is used to improve the grain boundary properties while Al and Cr are added to optimize the oxidation resistance. It has been reported that the mechanical properties of Ni-based superalloys are markedly influenced by crystallographic orientation [9,10]. So far, not much attention has been paid to the effect of crystallographic orientation on oxidation behavior of Ni-based single crystal superalloy. The main objective of this work is to investigate the influence of surface orientation on oxidation resistance of Ni-based single crystal superalloy at 1100 °C in air under isothermal condition.

2. EXPERIMENTAL DETAILS

A fully heat-treated CM186LC Ni-base single crystal superalloy was used as an experimental material. The chemical composition of superalloy in mass % is 5.74 Al, 0.73 Ti, 6 Cr, 9.3 Co, 1.4 Hf, 3.4 Ta, 2.9 Re, 8.3 W, 0.005 Zr, 0.016 B, 0.019 Fe, 0.07 C and balance Ni. For this purpose, a cylindrical rod of CM186LC superalloy was directionally solidified in [001]-direction. The rod was thermally heat-treated at 1080 °C for 4 h followed by gas fan cooling and then a single aging at 871 °C for 20 h completed by gas fan cooling. The principal oxidation surfaces of single-crystal samples were identified to be within 3° of the desired orientations using the Laue X-ray diffraction (XRD) technique. The specimens were then cut from the rod with the dimension of 10 mm in length, 5 mm in width and 3.5 mm in thickness with (001) and (011) surface orientations by electro discharge machine (EDM). Prior to isothermal oxidation, the specimens were mechanically polished down to 1200-grit SiC paper, degreased in acetone, ultrasonically cleaned in alcohol and dried in air.

Isothermal oxidation kinetic tests were performed at 1100 °C for 500 h in air environment. The oxidation kinetics was experimentally measured as a function of weight gain against exposure time. During oxidation, the weight gain of the specimens was quantified discontinuously. The sensitivity of the electron balance used in this study was 0.1 mg. The surface structure of CM186LC superalloy after oxidation was determined by X-ray diffraction (Rigaku) using Cu Kα radiation. The initial microstructure, surface morphology and cross-section of the CM186LC Ni-base single crystal superalloy after oxidation were analyzed by optical microscope (Olympus) and a JEOL scanning electron microscope equipped with energy-dispersive X-ray analysis (EDX).

3. RESULTS AND DISCUSSION

3.1. Initial microstructure

The optical and SEM micrographs of CM186LC superalloy are shown in Fig. 1 and Fig. 2, respectively. A Ni-base single crystal superalloy CM186LC contained 70–80% volume fraction of the γ′ phase.It is clearly seen two different areas which termed as dendritic and interdendritic as shown in Fig. 1. Dendritic areas consisted of γ′ precipitates which are uniformly distributed in the γ matrix

whereas the interdendritic areas generally contained γ′, γ′+γ eutectic precipitates in the γ matrix [11]. The configuration of dendrite structures was quite different between both surfaces where the dendrite structures were arranged in a perpendicular-like in (001) surface and the dendrite structures were formed an intersected-like of 45° in (011) surface. Meanwhile, Fig. 2 shows the cuboidal γ′ precipitates aligned along <001> during the aging treatment due to the elastic interaction between precipitates and its configurations in both surfaces.
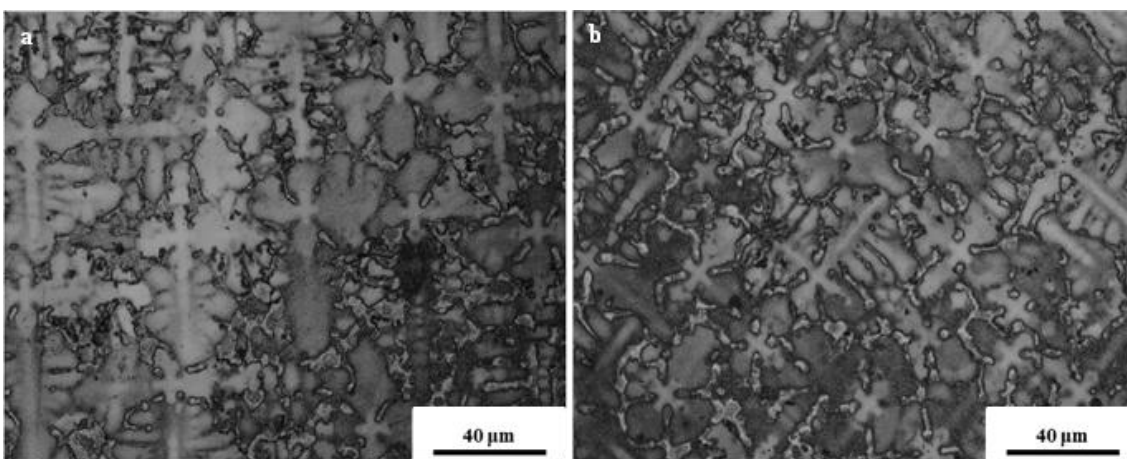
Figure 1. Optical micrographs of Ni-base single crystal superalloy CM186LC: (a) (001) surface and (b) (011) surface.
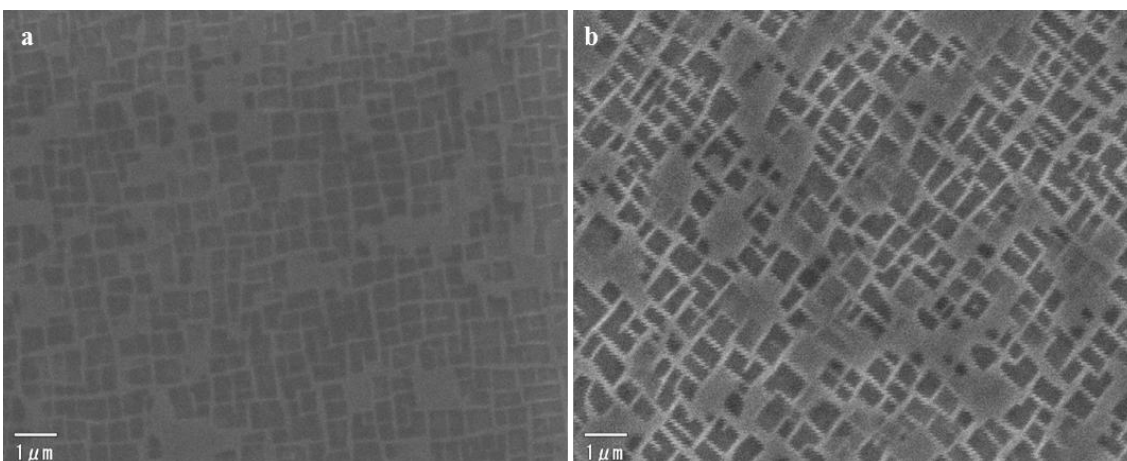

Figure 2. SEM micrographs of Ni-base single crystal superalloy CM186LC: (a) (001) surface and (b) (011) surface.

3.2. Oxidation kinetics

The curve of mass gain as a function of oxidation time at 1100°C is plotted in Fig. 3. The mass gain of the specimens in both surfaces was significantly increased in the first 25 h, this is due to the

free surface of superalloy. Afterwards, the mass gain of the specimens was gradually increased with increasing the oxidation time.
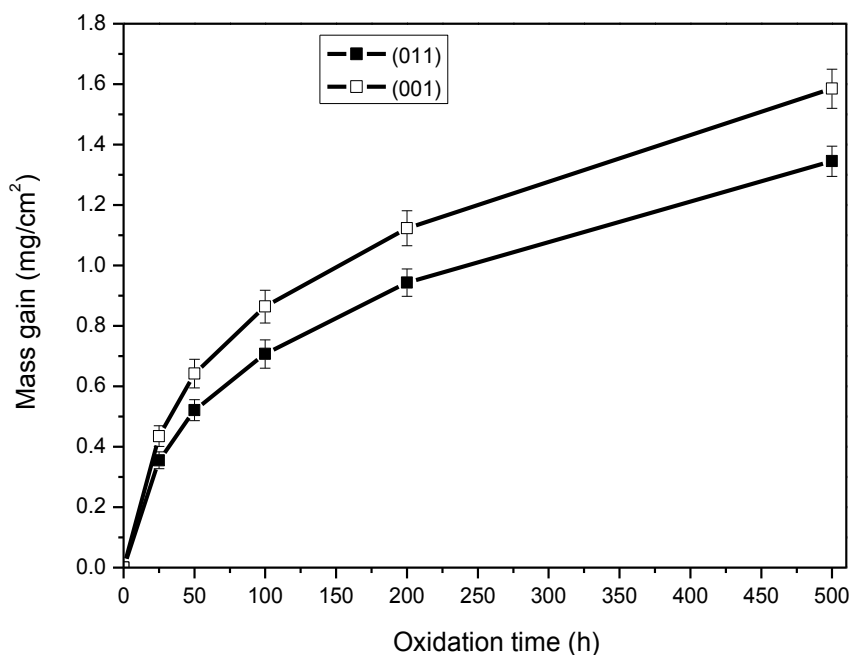
Figure 3. Oxidation kinetics curve of Ni-base single crystal superalloy CM186LC.
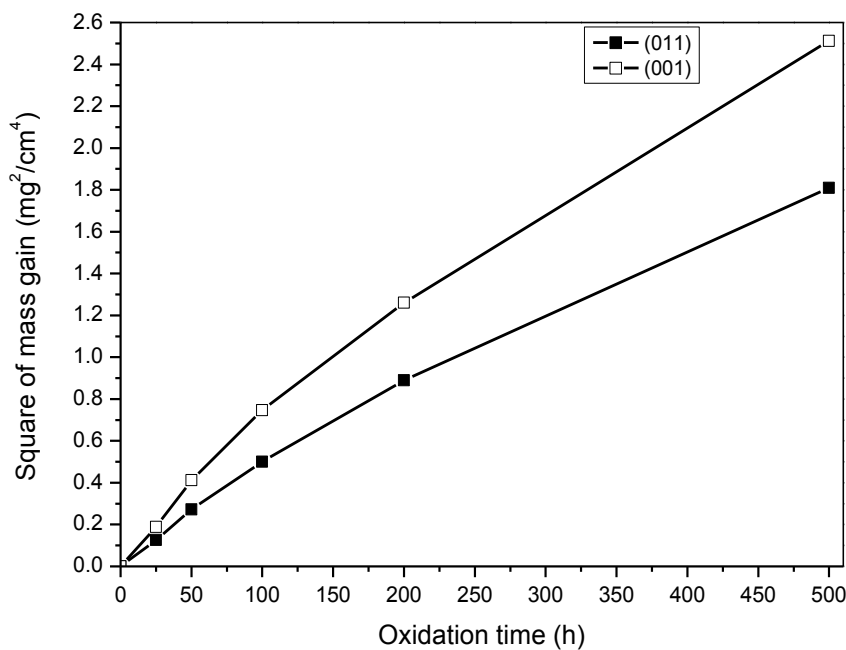
Figure 4. Square of the mass gain per unit area vs oxidation time for Ni-base single crystal superalloy CM186LC after oxidation in air at 1100°C.

As seen in Fig. 4, the plots of the square of mass gain obtained a nearly linear line which indicated that the oxidation kinetics followed a parabolic oxidation law at 1100°C. It was obvious that

the mass gain of specimens with (001) surface was higher than the specimens with (011) surface. Moreover, the parabolic rate constant K_p of superalloy can be estimated by a linear least-squares algorithm from the following equation [12]:

$$(\Delta m/A)^2 = K_p \cdot t \tag{1}$$

where K_p is the parabolic rate constant which can be directly obtained by plotting the square of the mass gain (mg^2/cm^4) over exposure time. The parabolic oxidation rate constants (K_p) and thus the oxidation rates of the superalloy in air are determined from the slope of $(\Delta m/A)^2$ vs t are 3.51×10^{-6} $mg^2cm^{-4}s^{-1}$ for (001) surface and 1.82×10^{-6} $mg^2cm^{-4}s^{-1}$ in (011) surface at 1100°C.

The oxidation kinetics of Ni-base single crystal superalloys in the temperature range of 800–1100°C in air has been reported which follows the parabolic law [13]. In the present study, the oxidation kinetics of Ni-base single crystal superalloy CM186LC nearly follows the parabolic law. The oxidation kinetics demonstrated that the specimens with (001) surface oxidized at rates more rapid than that the specimens with (011) surface and the curve shown in Fig. 3 represented this behavior. Furthermore, the parabolic oxidation rate (K_p) which derived from Fig. 4 exhibited that (001) surface has a higher oxidation rate than that of (011) surface. It means the anisotropy was also occurred on the oxidation behavior not only on the mechanical properties [10] of single crystal metals. In the other words, the oxidation behavior of single-crystal metals and alloys has been influenced by the crystallographic orientation of the specimen.
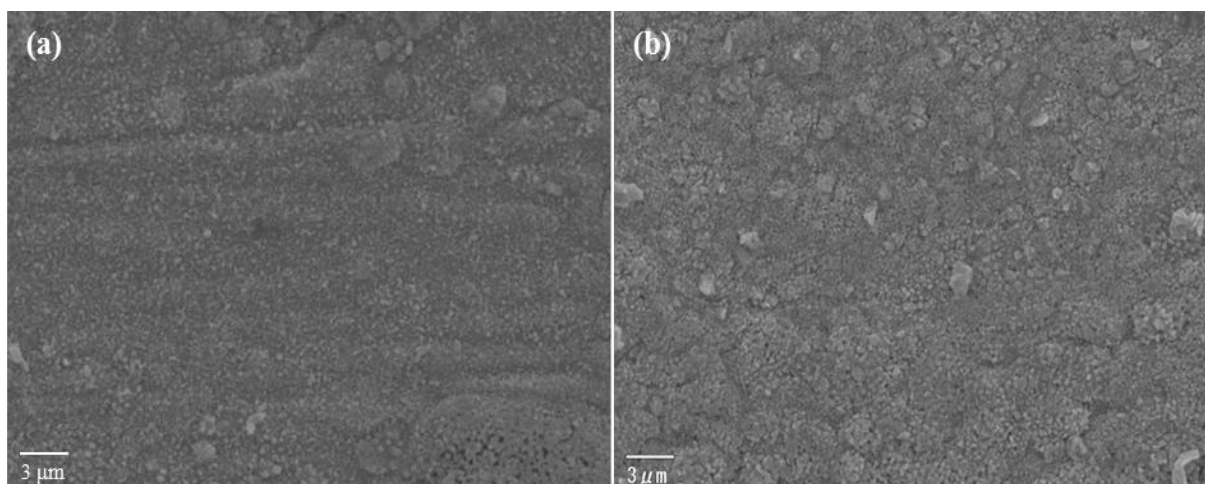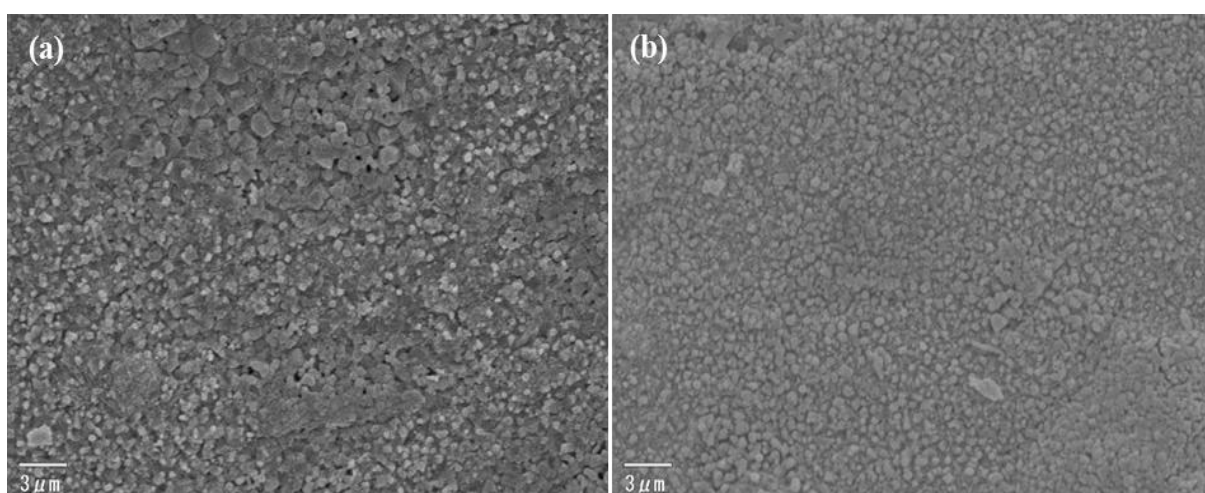
3.3. X-ray diffraction
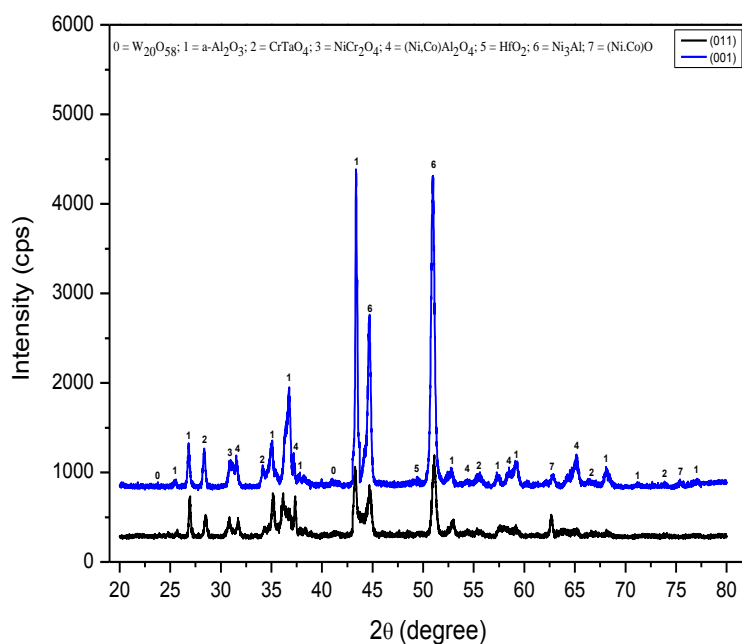
Figure 5. XRD patterns of Ni-base single crystal superalloy CM186LC after 500 h oxidation at 1100°C.

The results of X-ray diffraction of CM186LC Ni-base single crystal superalloys after 500 h oxidation at 1100°C are presented in Fig. 5. The oxide products formed on the suface of CM186LC superalloy were predominantly α-Al$_2$O$_3$ accompanied by spinels CrTaO$_4$, (Ni,Co)Al$_2$O$_4$ and some small amounts of (Ni,Co)O and HfO$_2$ were also detected. Basically, both surface orientations demonstrated a similar trend of peaks obtained. It was obvious that some peaks of oxide products on (001) surface exhibited higher intensity than that on (011) surface after 500 h oxidation. The difference in intensity of peaks may indicate that the anisotropy on the oxidation behavior was occurred due to different surface orientations of the specimens.
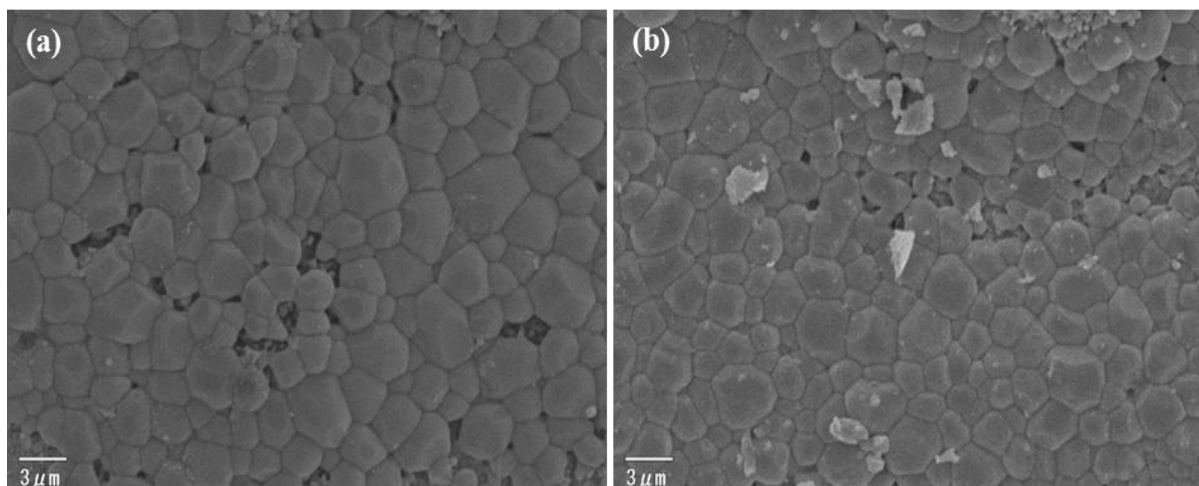
3.4. Surface morphology

Figure 6. Surface morphologies of Ni-base single crystal superalloy CM186LC after 25 h oxidation at 1100°C for: (a) (001) surface and (b) (011) surface.

Figure 7. Surface morphologies of Ni-base single crystal superalloy CM186LC after 100 h oxidation at 1100°C for: (a) (001) surface and (b) (011) surface.
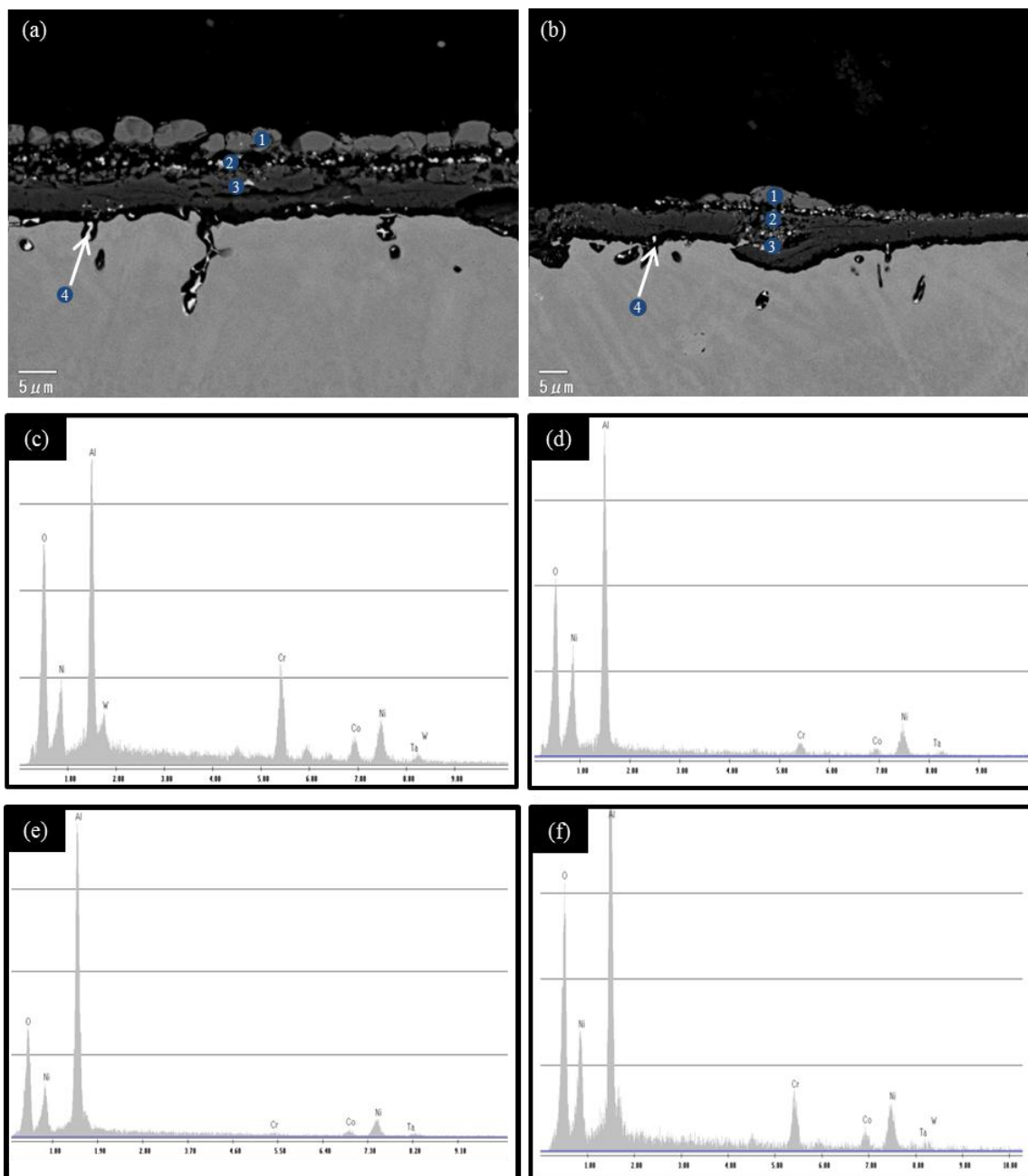
Figure 8. Surface morphologies of Ni-base single crystal superalloy CM186LC after 500 h oxidation at 1100°C for: (a) (001) surface and (b) (011) surface.

The oxide products formed on the surface of CM186LC single crystal superalloy was shown in Fig. 6-8. After 25 h oxidation, the oxide products formed has fine particle size with a high oxidation rate. The oxides were fully distributed on the surface of CM186LC superalloy on both orientations as shown in Fig. 6. Whereas the particles of oxides are being coarsened after 100 h oxidation as shown in Fig. 7. It was clear that the grain size of oxide particles increased with increasing the oxidation time. Meanwhile, the NiO particles were seen and spreaded over the surface of superalloy as seen in Fig. 8. However, NiO has a porous structure and blocky morphology. The grain size of NiO was varied between 0.71 μm to 5.94 μm on (001) surface and 0.64 μm to 4.45 μm on (011) surface.

3.5. Microstructure after oxidation

The SEM micrographs of cross-section back-scattered electron image (BEI) with the corresponding energy dispersive X-ray (EDX) of the scale formed on the CM186LC superalloy after 500 h oxidation at 1100°C are presented in Fig. 9. The BEI image was used in this investigation to enhance the atomic number contrast in the oxidation products. In general, the oxide scale formed on both surface orientations had a similar appearance but the configuration of oxide scale was somewhat different on both surface orientations as shown in Fig. 9. Hence, the surface orientations seem not only affect the oxidation kinetics, but also influence the configuration of oxide scale developed on the surfaces of superalloy when oxidized at elevated temperatures. Overall, the oxide scale on both surfaces consisted of an outer layer was made of NiO layer with a small amount of CoO (point 1), an intermediate layer (points 2 and 3) and inner layer was composed of α-Al_2O_3 continuous layer which appeared as dark areas at the bottom of oxide scale combined with a small amount of HfO_2 precipitate (point 4) as shown in Fig. 9a and 9b. For (001) surface, the intermediate layer can be divided into two layers, the first layer mainly composed of $(Ni,Co)Al_2O_4$, $CrTaO_4$, $NiCr_2O_4$ with a small amount of $W_{20}O_{58}$ (point 2), whereas the second one mainly composed of $(Ni,Co)Al_2O_4$, $NiCr_2O_4$ with a small amount of $CrTaO_4$ (point 3). Meanwhile for (011) surface, the first intermediate layer predominantly

consisted of $(Ni,Co)Al_2O_4$ with a small amount of $CrTaO_4$ and $NiCr_2O_4$ (point 2), whereas the second intermediate layer predominantly consisted of $(Ni,Co)Al_2O_4$, $NiCr_2O_4$, $CrTaO_4$ with a small amount of $W_{20}O_{58}$.

Figure 9. Cross-sectional SEM images of Ni-base single crystal superalloy CM186LC after 500 h oxidation at 1100°C: (a) (001) surface and (b) (011) surface; (c) to (f) represent the corresponding EDX profile analysis derived from the intermediate layer (points 2 and 3): (c) and (e) for micrograph shown in (a) whereas (d) and (f) for micrograph shown in (b).

The detailed EDX result of the specimens after 500 h oxidation at 1100°C was summarized in Table 1. Moreover, the thickness of oxide scale increased by extending the oxidation time to be about
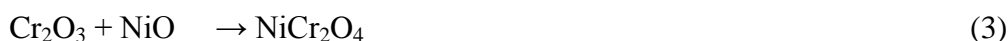
9.77 μm to 14.78 μm for (001) surface and 5.87 μm to 11.84 μm for (011) surface as shown in Fig. 9. The EDX results were consistent to the XRD pattern obtained. The difference in thickness of oxide scale exhibited that the anisotropy on oxidation behavior was occurred which proved that the crystallographic orientation influenced the oxidation behavior of Ni-base single crystal superalloy.

Table 1. Chemical content of main elements in typical phase zone (at.%) in Fig. 9

Condition	Points of no.	Element content (at.%)								Note
		O	Ni	Al	Cr	Co	Ta	W	Hf	
1100°C/500 h in (001) surface (Fig. 8a)	1	28.24	62.28	-	-	9.48	-	-	-	NiO+CoO
	2	39.42	13.64	25.5	12.77	6.2	1.75	0.72	-	$(Ni,Co)Al_2O_4+NiCr_2O_4+CrTaO_4+W_{20}O_{58}$
	3	38.27	25.92	24.08	6.21	4.85	0.67	-	-	$(Ni,Co)Al_2O_4+NiCr_2O_4+CrTaO_4$
	4	53.23	0.34	40.38	0.98	0.79	-	-	3.28	$\alpha-Al_2O_3+HfO_2$
1100°C/500 h in (011) surface (Fig. 8b)	1	37.59	56.26	-	-	6.15	-	-	-	NiO+CoO
	2	46.18	13.71	34.24	2.45	2.38	1.05	-	-	$(Ni,Co)Al_2O_4+NiCr_2O_4+CrTaO_4$
	3	41.18	14.36	31.46	6.61	4.19	1.77	0.43	-	$(Ni,Co)Al_2O_4+NiCr_2O_4+CrTaO_4+W_{20}O_{58}$
	4	51.65	0.74	43.47	0.87	0.35	-	-	2.92	$\alpha-Al_2O_3+HfO_2$

3.6. Formation of oxide scales

Mostly, the simple oxides such as NiO, CoO, Al_2O_3 and others are formed during the initial oxidation stage but the transient-oxidation period was very short because of the rapid build-up of the inner $\alpha-Al_2O_3$ resulting from rapid outward diffusion of Al in the superalloy. A mixed-oxide scale formed on the surface of CM186LC superalloy after 500 h oxidation at 1100°C. The solid phase reaction among the simple oxides may occur, leading to the formation of $(Ni,Co)Al_2O_4$ [14], $NiCr_2O_4$ [15] and $CrTaO_4$ [16] as described in the following reactions:

$$(Ni,Co)O + Al_2O_3 \rightarrow (Ni,Co)Al_2O_4 \qquad (2)$$

$$Cr_2O_3 + NiO \rightarrow NiCr_2O_4 \qquad (3)$$

$$Cr_2O_3 + Ta_2O_5 \rightarrow CrTaO_4 \qquad (4)$$

Besides, the HfO_2 precipitates are visible decorating within the inner $\alpha-Al_2O_3$ as mentioned in Table 1. HfO_2 precipitate [17] was produced by the following reaction:

$$HfC + O_2 \rightarrow HfO_2 + CO_2 \qquad (5)$$

A low content of (Ni,Co)O is still observed after 500 h oxidation at 1100°C as shown in Fig. 10. This is due to the rapid consumption of (Ni,Co)O resulted from the formation of $(Ni,Co)Al_2O_4$ by the acceleration of solid-state diffusion reaction between the transient NiO and $\alpha-Al_2O_3$ at high temperature. The extension of oxidation time results in the increasing the thickness of the oxide scales which causes the change in chemical composition of its oxides. The NiO grew become larger forming

a blocky morphology as seen in Fig. 8a and 8b. Moreover, Ni diffusion outward is hindered by the rapid development of the inner α-Al_2O_3 layer, and NiO growth is finally inhibited.

3.7. Anisotropy on oxidation behavior

The oxidation kinetics curve (Fig. 3) shows that the anisotropy on oxidation behavior was occurred where the specimens with (001) surface has a higher oxidation rate value than that of the specimens with (011) surface as shown in Fig. 4. The results obtained in this study is consistent with the previous works where the relationship (111) < (011) < (001) was observed for oxidation of Nickel single crystal [18]. Scales formed in the initial stage should be oriented with respect to the substrate, and then a transition to a randomly-oriented scale occurs. It could be realized that after a long oxidation time, the oxide scale is too thick to retain its growth epitaxially. Consequently, the degree of preferred oxide orientation decreases with increasing the oxidation time. It is considered that this oxidation anisotropy is mainly due to the effect of short-circuit diffusion paths on both surfaces. The difference of the mosaic structure changing the extent of the short-circuit diffusion paths where they play an important role as a function of the crystallographic orientations of the single crystal surfaces. Therefore, the specimen surfaces with different crystallographic orientations exhibit various oxidation rates [19]. When the oxidation scales grow on the surface of Ni-based superalloy, they contains a large number of short-circuit diffusion paths. The specimens with (001) surface has larger number of diffusion paths than the specimens with (011) surface. These short circuit diffusion paths are frequently generated because the oxide scale is subjected to an epitaxial-growth force during its growth on surfaces of single crystal alloys during isothermal oxidation [20,21]. It has also been confirmed that the oxides grown on the (001) surface produce more grain boundaries if compared with the (011) surface because the specimen with (001) surface has four possibilities of the oxide alignments [19,22]. A higher concentration of grain boundaries may promote higher diffusivities than the bulk [23] and they seem to be responsible for the differences in oxidation rate.

Another approach can be used to verify the anisotropy on oxidation behavior of superalloy CM186LC that is by measuring and then comparing the thickness of oxide scale formed on the surface of superalloy between the two orientations. The difference in the oxide scale thickness was apparent where the maximum thickness of oxide scale formed is about 14.78 μm on (001) surface and 11.84 μm on (011) surface after 500 h oxidation. This occurrence is due to the specimens with (001) surface has a higher K_p value than the specimens with (011) surface.

4. CONCLUSIONS

Based on the experimental investigation, the following conclusions can be withdrawn:

(i) The oxidation kinetics characteristic of Ni-base single crystal superalloy CM186LC at 1100°C follows the parabolic law which is controlled predominantly by the growth of the inner α-Al_2O_3 layer.

(ii)   The specimens with (001) surface exhibits a higher K_p value than the specimens with (011) surface which indicated that the anisotropy on oxidation resistance was occurred between the two surface orientations. In addition, the surface orientation of the specimens influenced the oxidation resistance of Ni-base single crystal superalloy CM186LC.

(iii)   The anisotropy on oxidation resistance mainly caused by the different of short-circuit diffusion paths between the two surfaces where can be realized from the difference in K_p values obtained which means the (001) surface has a larger number of diffusion paths than that on (011) surface. The difference in K_p values resulted in the difference in the thickness of oxide scales obtained on the surface of superalloy CM186LC during isothermal oxidation.

References

1. D. W. MacLachlan, D. M. Knowles, *Mater. Sci. Eng. A.*, 302 (2001) 275.
2. J. S. Bae, J. H. Lee, S. S. Kim, C. Y. Jo, *Script. Mater.*, 45 (2001) 503.
3. K. Shirvani, M. Saremi, A. Nishikata, T. Tsuru, *Corros. Sci.*, 45(5) (2003) 1011.
4. B. Pieraggi, F. Dabosi, *Mater. Corros.*, 38 (1987) 584.
5. M. H. Li, X. F. Sun, T. Jin, H. R. Guan, Z. Q. Hu, *Oxid. Met.*, 60 (2003) 195-210.
6. G. E. Fuchs, *Mater. Sci. Eng. A.*, 300 (2001) 52.
7. H. Zhou, Y. Ro, H. Harada, Y. Aoki, M. Arai, *Mater. Sci. Eng. A.*, 381 (2004) 20.
8. N. Czech, F. Schmitz, W. Stamm, *Surf. Coat. Technol.*, 68/69 (1994) 17.
9. M. B. Henderson and J. W. Martin, *Acta Mater.*, 44 (1996) 111.
10. V. Sass, V. Glatzel, and M. Feller-Kniepmeier, *Acta Mater.*, 44 (1996) 1967.
11. B. Dubiel and A. Czyrska-Filemonowicz, *J. Microscopy*, 224 (2006) 8.
12. B. Wang, C. Sun, J. Gong, R. Huang, L. Wen, *Corros. Sci.*, 46 (2004) 519.
13. T. F. An, H. R. Guan, X. F. Sun and Z.Q. Hu, *Oxid. Met.*, 54 (2000) 301.
14. B. Pieraggi, *Mater. Sci. Eng.*, 88 (1987) 199.
15. K. Hauffe, G.H. Meier, Oxidation of Metals, Plenum, New York, 1966.
16. O. Kubaschewski, B.E. Hopkins, Oxidation of Metals and Alloys, Butterworths, London, 1962.
17. Per Kofstad, High Temperature Corrosion, Elsevier Applied Science, London and New York, 1988.
18. C.A. Schuh, K. Anderson, C. Orme, *Surf. Sci.*, 544 (2003) 183.
19. J.V. Cathcart, G.F. Petersen, and C. J. Sparks, Jr, *J. Electrochem. Soc.*, 116 (1969) 664.
20. J.V. Cathcart and G.F. Petersen, *J. Electrochem. Soc.*, 115 (1968) 595.
21. B.S. Borie, C.J. Sparks, Jr and J.V. Cathcart, *Acta Metall.*, 10 (1962) 691.
22. N.N. Khoi, W. W. Smeltzer, J. D. Embury, *J. Electrochem. Soc.,* 122 (1975) 1495.
23. H. Li, F. Czerwinski, A. Zhilyaev, J.A. Szpunar, *Corros. Sci.*, 39 (1997) 1211.